CHARACTERISTICS OF A COMPRESSIBLE BACKWARD-FACING STEP FLOW

Kung-Ming Chung
Aerospace Science and Technology Research Center
National Cheng Kung University
1 University Road, East, Tainan, 701, Taiwan
kmchung@mail.ncku.edu.tw

Kao-Chun Su
Department of Mechanical Engineering
National Yunlin University of Science and Technology
123 University Road Section 3, Douliou, Yunlin, 640, Taiwan
sukc@yuntech.edu.tw

ABSTRACT

Turbulent flow past a backward-facing step is characterized by shear layer separation, recirculation, reattachment and a redeveloping boundary layer. This study uses dynamic pressure measurements to determine the distribution of the mean and fluctuating pressures for a two-dimensional backward-facing step at high subsonic speeds. The peak pressure fluctuations have a value of 5-6% of the freestream dynamic pressure. The location for reattachment (5.1-6.1 step height) and extra reattachment (0.9-2.0 step height) is determined using the oil flow visualization. The effect of step height (for strong perturbation) and freestream Mach number on the characteristic non-dimensional frequencies is determined. A broadband dominant peak, which corresponds to shear layer or vortex shedding mode, is the dominant factor in intensive pressure fluctuations.

INTRODUCTION

Flow separation and reattachment is important for the design and control of many practical engineering configurations (Eaton and Johnston, 1981). A backward-facing step (BFS) is a simple geometric discontinuity (airfoil, vehicles or building). For a BFS flow, Fig. 1 shows that a boundary layer separates at the edge of the step. There are tiny spanwise vortices in the first part of the very thin, curved shear layer and thicker vortices during convection downstream due to Kelvin-Helmholtz instabilities (Bradshaw and Wong, 1972). The shear layer impinges on the bottom wall and splits at the reattachment location. The mean reattachment location is denoted as x_r (= 3.0–8.5 H) (Park et al., 2007; Scharnowski et al., 2015; Rusi et al., 2016; Hu et al., 2021). The upstream flow entrains the primary circulation under the shear layer and the downstream flow relaxes to a redeveloping boundary layer (Chen et al., 2018). The bottom portion of the primary vortex travels upstream and the secondary circulation (vortex that is counter-rotational to the primary vortex) forma a roughly triangular region near the step. Schrijer et al. (2014) determined that the size of the secondary recirculation region decreases as the Reynolds number increases. The recirculation region is characterized by lower pressure than the freestream conditions, which induces greater base drag (Deck and Thorigny, 2007). The primary–secondary vortex interface is denoted as the extra reattachment, x_s (Hall et al., 2003).

The turbulent separated shear layer for a high subsonic flow over a BFS can result in intense pressure fluctuations and the effect of H^* is not known. An experimental study is conducted for a BFS flow (H = 3, 5 and 7 mm; a strong perturbation), for which the values of freestream Mach number M are 0.30, 0.60 and 0.81. Oil flow visualization is used to determine the location of the mean and the extra reattachment. Dynamic pressure measurements are used to determine the mean and fluctuating pressure distributions.

EXPERIMENTAL SETUP

Transonic wind tunnel

The experimental tests were performed in a transonic wind tunnel at the Aerospace Science and Technology Research Center of National Cheng Kung University (ASTRC/NCKU). The tunnel is a blowdown type. Three storage tanks (total volume = 180 m^3 operating at a maximum pressure of 5.15 MPa) with two compressors and two air dryers supply dry high-pressure air (dew point ≈ −40 °C). A rotary perforated sleeve valve controls the stagnation pressure, p_o, and pressurized air is discharged into a stilling chamber, in which acoustic baffles, screens, and a honeycomb reduce noise and turbulence intensity of the flow. The square constant-area test section has perforated top and bottom walls (6% porosity) and solid side walls and has a cross-section of 600x600 mm^2 and a length of 1500 mm. The freestream Mach number, M, is monitored using a nozzle and two choke flaps downstream of the test section. A divergent subsonic diffuser decelerates the flow that exhausts to the atmosphere. The value of p_0 is 172±0.5 kPa, and the stagnation temperature is room temperature. The value of M is 0.30, 0.60 and 0.81±0.01 where the uniformity in the streamwise direction is approximately 0.005. The corresponding Reynolds numbers are 1.08, 1.93 and 2.31 × 10^7 per meter. The test conditions are recorded using a National Instruments system (Austin, TX, USA), including PXIe-8840 RT, PXI-7846, PXI-6511, and PXI-6513 NI-SCXI.

Test model and instrumentation

Fig. 2 shows a schematic diagram of the test model, which comprises a flat plate and an instrumentation plate with a BFS. The model is supported by a single sting that is mounted on the bottom wall of the test section. The flat plate is 450 mm long and the interchangeable instrumentation plate is 170 mm long. The width of the model, W, is 150 mm. The step (H = 3, 5 and 7 mm) is located 500 mm from the leading edge of the flat plate. Two side fences are also installed to prevent crossflow. The value of W/H ranges from 24.3 to 56.7 to avoid 3-D effects (de Brederode and Bradshaw, 1972).

A turbulent boundary layer develops naturally along the flat plate. Normalized velocity profiles are full (n ≈ 7-11 for the velocity power law) (Chung, 2000). The value of the boundary layer thickness, δ, at 25 mm upstream of the BFS is 8.3 mm for M = 0.30, 7.4 mm for M = 0.60 and 7.1 mm for M = 0.81. The value of H^* is 0.36-0.84 for M = 0.30, so the value is 0.42-0.99 for M = 0.60 and 0.81 (a strong perturbation) (Bradshaw and Wong, 1972).

Surface pressure fluctuations in turbulent flows are associated with a surface excitation force and noise generation. Measurements of surface pressure fluctuations are required for a BFS flow. Nineteen pressure taps are drilled perpendicular to the model surface in the streamwise direction. Kulite pressure transducers (XCS-093-25A, a B screen with a natural frequency of 200 kHz; Leonia, NJ, USA) are potted using silicone rubber sealant and are flush-mounted to measure the mean and fluctuating surface pressure. These Kulite sensors are powered by a TES Model 6102 power supply that operates at 10.0 V. Gramann and Dolling (1990) showed that the frequency response for a Kulite pressure transducer due to the perforated screen is approximately 50 kHz. These Kulite sensors have low-pressure sensitivity. In this context, external amplifiers (Ectron Model E713; San Diego, CA, USA) with a gain of 20 (roll-off frequency ≈ 140 kHz) are used to improve the signal-to-noise ratio. A National Instruments system (CI SCXI; Austin, TX, USA) records data at a sampling rate of 200 kHz (5 μs).

Each pressure-history contains 131,072 data points. The data is divided into 32 blocks for data processing. The experimental uncertainty is 0.62% for the mean surface pressure coefficient, C_p (= $(p_w-p_\infty)/q$), and is 0.15% for the surface fluctuating pressure coefficient, C_{σ_p} (= $(\sigma_p-\sigma_{p,\infty})/q$). The respective static and fluctuating pressures for a flat-plate flow are p_∞, $\sigma_{p,\infty}$ (rms pressure) and q denotes inflow dynamic pressure. It is also noted that the respective discrete tones due to the top and bottom perforated walls for M = 0.60 and 0.81 occur at frequencies of approximately 4200 and 4700 Hz (Chung et al., 2013).

This study uses oil-flow visualization. A compound mixture of titanium dioxide, oil, and oleic acid is applied to the surface of the instrumentation plate. An accumulation of titanium dioxide signifies extra reattachment between the primary and secondary circulations. The end of the deflected streak line denotes shear layer reattachment. The mean position for x_R and x_S is determined.

RESULTS AND DISCUSSION

Surface oil flow visualization

The location for extra reattachment and reattachment downstream of the step is determined using surface oil flow visualization. An example (M = 0.81 and H^* = 0.99) is shown in Fig. 3. The beginning of accumulation is defined as the interface between the primary and the secondary vortex (extra reattachment) and the end of deflection is denoted as the mean location for reattachment.

Fig. 4 shows the length of extra reattachment. Tihon et al. (2001) showed that there is a stable secondary circulation region for low Reynolds numbers, but not true for the test conditions for this study. The value for x_s/δ or x_s/H at M = 0.30 is greater than that at M = 0.60 and 0.81 and the value of H has an effect. The value of x_s/δ or x_s/H for H = 3 mm is greater than that for H = 5 and 7 mm. In this context, there is an extension of the secondary corner vortex and the bottom portion of the primary vortex travels less upstream towards the step corner for H = 3 mm.

Eaton and Johnston (1981) determined that the streamwise extension of the primary recirculation region depends primarily on the value of H and Bolgar et al. (2018) showed that the mean reattachment location from a subsonic to a transonic flow regime moves downstream. A summary of the reattachment length is shown in Fig. 5. The value of x_r/δ increases as M and H increase. There is a minor increase in the value of x_r/H as M increases. The value of x_r/H ranges from 5.1 to 6.1 which is similar to the results of previous studies (Eaton and Johnston, 1981; Scharnowski et al., 2015). This also shows that H has a smaller effect on the value of x_r/H.

Distribution of mean surface pressure

The distribution of C_p for H = 3 mm is shown in Fig. 6. The horizontal axis is the normalized streamwise location, x^* (= x/δ), and the origin is the edge of the step. Upstream influence is demonstrated by the presence of the step, particularly for M = 0.30. The minimum value for C_p, $C_{p,min}$, is measured at x^* = 1.1-1.3 which is near the interface between the primary and secondary vortex. There is a significant and rapid increase in pressure toward the reattachment position. The shear layer is deflected upstream into the recirculating flow. The peak C_p value is achieved downstream of the mean reattachment location (x^* = 4.0-5.5). An increase in M results in an extension of the recompression process, which is similar to the effect of M on x_r. The wall pressure decreases downstream of the reattachment location and gradually returns to its initial value ($C_p \approx 0$).

The recirculation region is a region of low pressure so there is an increase in base drag. There is variation in the value of $C_{p,min}$ as shown in Fig. 7. For M = 0.30, an increase in H^* increases the value of $C_{p,min}$ but the value decreases as H^* increases for M = 0.60 and 0.81. There is a significant decrease in the value of $C_{p,min}$ as H^* increases, particularly for M = 0.80. There is significantly greater base drag for a BFS at high subsonic speeds.

Fluctuating pressure

The distribution of the fluctuating pressure coefficient for H = 3 mm is shown in Fig. 8. There is a minor variation in the amplitude of $\boldsymbol{C_{\sigma_p}}$ upstream of the step, an increase toward the reattachment location and a recovery process toward that of the freestream condition at locations that are further downstream. Lee and Sung (2001) determined that the amplitude of $\boldsymbol{C_{\sigma_p}}$ for a BFS flow has a maximum value slightly upstream of the reattachment location because there are large-scale vortices (shedding vortices). This agrees with the results of the current study, except for M = 0.30. Pressure fluctuations are slight for M = 0.30, so the data for this condition must be treated with caution.

Bolgar et al. (2018) determined that the step mode is the primary source of pressure fluctuations in a subsonic flow regime and the gradient of pressure fluctuations is very steep around the maximum point. Deck and Thorigny (2007) showed that large-scale vortical motion persists after reattachment, so the surface pressure fluctuations decrease slowly after reattachment. For H = 5 mm, Fig. 9 shows that the value of C_{σ_p} is negative upstream of the step. The location for the maximum value for C_{σ_p}, $C_{\sigma_{p,peak}}$, moves downstream (x^* = 3.25-3.80) as M increases, which agrees with the data for x_r, as shown in Fig. 5. These results also show that there is a gradual decrease in the value of C_{σ_p} toward downstream locations. The distribution for H = 7 mm, as shown in Fig. 10, is similar to that for H = 5 mm. There is a slow downstream recovery process as the value of H increases.

Deck and Thorigny (2007) summarizes a flow data set that features flow reattachment. For a BFS on a revolving body at M = 0.7 and 0.8, the value of the ratio between the peak rms pressure and q, $\sigma_{p,max}/q$, is 0.05-0.07. Fig. 11 shows the variation in $\sigma_{p,max}/q$ for M = 0.60 and 0.81. The value is 0.05-0.06 which shows that the oscillation in the reattachment location (step mode) is similar for a 2D BFS and a BFS on a revolving body. There is also an increase in the value of $\sigma_{p,max}/q$ as H^* (= 0.41-0.70) increases, but not for greater values of H^*. For H^* = 0.41-0.70, the value of $\sigma_{p,max}/q$ for M = 0.81 is greater than that for M = 0.60.

Intense pressure fluctuations can excite a response in the structural modes and can cause acoustic problems. For a BFS flow, the flapping motion of the shear layer results in a periodic change for the location for reattachment. The study by Lee and Sung (2001) determined that the frequency is low frequency for an incompressible BFS flow for which the Strouhal number St_H is approximately 0.01-0.015 or $St_{x_r} \approx$ 0.11. For M = 0.81, Fig. 12a shows that the value of St_H is 0.006 for $H^* \approx$ 0.42 and 0.011 for H^* = 0.70 and 0.99. This value is 0.011 for M = 0.60 and H^* = 0.68, but not for H^* = 0.41 and 0.95 ($St_H \approx 0.008$). Fig. 12b shows that the value of St_{x_r}(= 0.047-0.029) decreases for M = 0.60 and increases for M = 0.81 (St_{x_r}= 0.037-0.04) as H^* increases. The effect of compressibility requires further study.

Simpon (1989) (a 2D BFS in incompressible flow) determined the value of St_{x_r} ($\approx$ 0.6-0.8) for the vortex shedding mode and a similar result ($St_{x_r} \approx$ 0.6) was reported by Deck and Thorigny (2007) (for an axisymmetric step flow at M = 0.702). Fig. 13a shows the effect of H^* on the variation in St_H (= 0.045-0.108), which is similar to the effect on the variation in the step mode. For a specific value of H^*, the value of St_H for M = 0.60 is greater than that for M = 0.81. For M = 0.60 and H^* = 0.68, Fig. 13b shows that the value of $St_{x_r}$is 0.61 which is similar to the value that is calculated by previous studies. There is a significant decrease ($St_{x_r} = 0.38$) for $H^* \approx$ 0.41. For M = 0.81, the value of $St_{x_r}$is less than that for M = 0.60. There is also a lower value for H^* = 0.42 (St_{x_r}= 0.27).

CONCLUSIONS

Oil flow visualization shows that the mean reattachment location for the separated shear layer moves downstream as the step height and the freestream Mach number increase. The non-dimensional reattachment location (x_r/H) varies from 5.1 to 6.1, and the effect of H is less significant. The interface between the primary and secondary vortex (extra reattachment) is also visualized. There is an extension of the secondary corner vortex for a smaller step, for which the bottom portion of the primary vortex travels less upstream towards the step corner.

The distribution of the mean surface pressure coefficient demonstrates upstream influence in the presence of a step. Low pressure in the recirculation region creates an increase in base drag. There is a significant decrease in the value of the minimum surface pressure coefficient as the ratio between the step height and boundary layer thickness increases. There is a rapid and significant pressure increase toward the reattachment position and the maximum value occurs downstream of the mean reattachment location. The location of the maximum surface pressure coefficient moves downstream as the height of the step increases.

Noise and vibration that are induced by turbulence have a significant impact on vehicle structures. There is a maximum fluctuating pressure coefficient (= 5-6% freestream dynamic pressure at high subsonic speeds) slightly upstream of the reattachment location and this location moves downstream as the freestream Mach number increases. The characteristic non-dimensional frequencies vary with the step height and the freestream Mach number. The effect of compressibility on the characteristic frequencies requires further study.

REFERENCES

Eaton, J.K. and Johnston, J.P., 1981, "A Review of Research on Subsonic Turbulent Flow Reattachment“, *AIAA Journal*, Vol. 19, pp. 1093-1110.

Bolgar, I., Scharnowski, S. and Kähler, C.J., 2018, "The Effect of the Mach Number on a Turbulent Backward-Facing Step Flow“, *Flow, Turbulence and Combustion*, Vol. 101, pp. 653–680.

Bradshaw, P. and Wong, F.Y.E., 1972, "The Reattachment and Relaxation of a Turbulent Shear Layer“, *Journal of Fluid Mechanics*, Vol. 52, pp. 113-135.

Chen, L., Asai, K., Nonomura, T., Xi, G. and Liu, T., 2018, "A Review of Backward-Facing Step (BFS) Flow Mechanisms, Heat Transfer and Control“, *Thermal Science and Engineering Progress*, Vol. 6, pp. 194-216.

Chung, K.M., 2000, "Transition of Subsonic and Transonic Expansion-Corner Flows“, *Journal of Aircraft*, Vol. 37, No. 6, pp. 1079-1082.

Chung, K.M., Chang, P.H. and Chang, K.C., 2013, "Tunnel Background Noise on Compressible Convex-Corner Flows“, *Journal of Aircraft*, Vol. 50, No. 4, pp. 1011-1015.

de Brederode, V. and Bradshaw, P., 1972, "Three-Dimensional Flow in Nominally Two-Dimensional Separation Bubbles“, I: Flow behind a rearward facing step. Report. Imperial College of Science and Technology, IC Aero, 72–19.

Deck, S. and Thorigny, P., 2007, "Unsteadiness of an Axisymmetric Separating-Reattaching Flow: Numerical Investigation“, *Physics of Fluids*, Vol. 19, 065103

Gramann, R.A. and Dolling, D.S., 1990, "Detection of Turbulent-Boundary Layer Separation Using Fluctuating Wall Pressure Signals“, *AIAA Journal*, Vol. 28, No. 6, pp. 1052-1056.

Hall, S.D., Behnia, M., Fletcher, C.A.J. and Morrison, G.L., 2003, "Investigation of the Secondary Corner Vortex in a Benchmark Turbulent Backward-Facing Step Using Cross-Correlation Particle Imaging Velocimetry“, *Experiments in Fluids*, Vol. 35, pp. 139-151.

Hu, W., Hickel, S. and van Oudheusden, B.W., 2021, "Low-Frequency Unsteadiness Mechanisms in Shock Wave/Turbulent Boundary Layer Interactions over a Backward-Facing Step“, *Journal of Fluid Mechanics*, Vol. 915, A107.

Lee, I. and Sung, H.J., 2001, "Characteristics of Pressure Fluctuations in Separated and Reattaching Flow over a Backward-Facing Step: Part I. Time-Mean Statistics and Cross-Spectral Analyses“, *Experiments in Fluids*, Vol. 30, pp. 262-272.

Park, H., Jeon, W.P., Choi, H. and Yoo, J.U., 2007, " Mixing Enhancement behind a Backward Facing Step Using Tabs“, *Physics of Fluids*, Vol. 19, 105103.

Ruisi, R., Zare-Behtash, H., Kontis, K. and Erfani, R., 2016, "Active Flow Control over Backward-Facing Step

Using Plasma Actuation“, *Acta Astronautica*, Vol. 126, pp. 354-363.

Scharnowski, S., Bolgar, I. and Kahler, C.P., 2015, "Control of the Recirculation of aTtransonic BFS Flow Using Circular Lobes“, *International Symposium on Turbulence and Shear Flow Phenomena*,. Melbourne, Australia.

Schrijer, F.E.J., Sciaacchitano, A. and Scarano, F., 2014, "Spatio-Temporal and Modal Analysis of Unsteady Fluctuations in a High-Subsonic Base Flow“, *Physics of Fluids*, Vol. 26, 086101.

Simpson, R.L., 1989, "Turbulent Boundary-Layer Separation“, *Annal Review in Fluid Mechanics*, Vol. 21, pp. 205–232.

Tihon, J., Legrand, J. and Legentilhomme, P., 2001, "Near-Wall Investigation of Backward-Facing Step Flows“, *Experiments in Fluids*, Vol. 31, Issue 5, pp. 484–493.

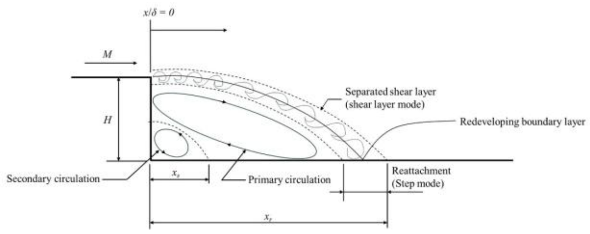

Figure 1. A schematic diagram of a BFS flow.

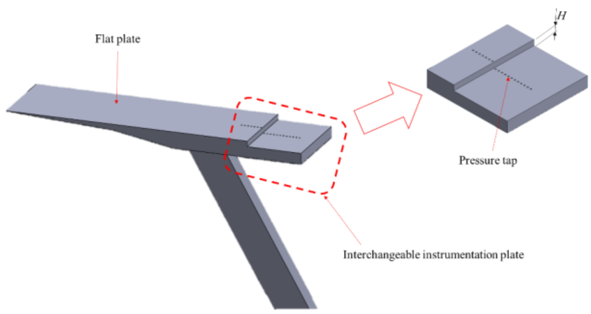

Figure 2. Test configuration.

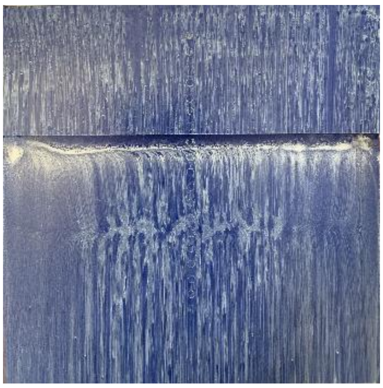

Figure 3. Surface oil flow visualization for M = 0.81 and H^* = 0.99.

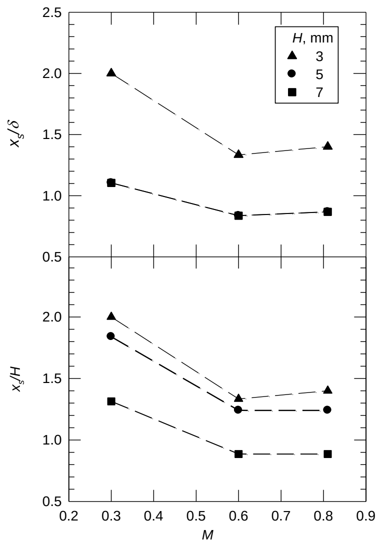

Figure 4. Length for extra reattachment.

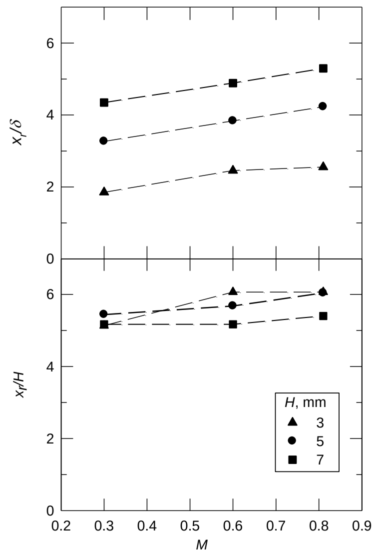

Figure 5. Reattachment length.

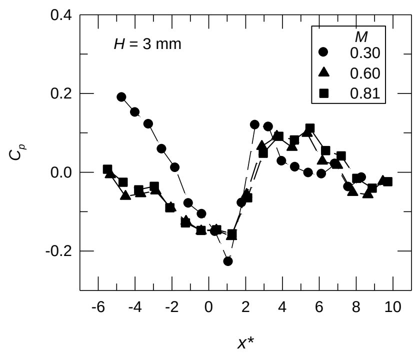

Figure 6. Distribution of surface pressure coefficient for H = 3 mm.

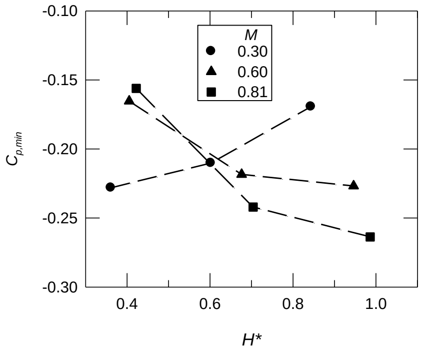

Figure 7. Minimum surface pressure coefficient.

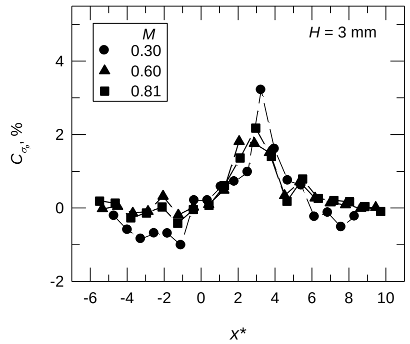

Figure 8. Distribution of fluctuating pressure coefficients for H = 3 mm.

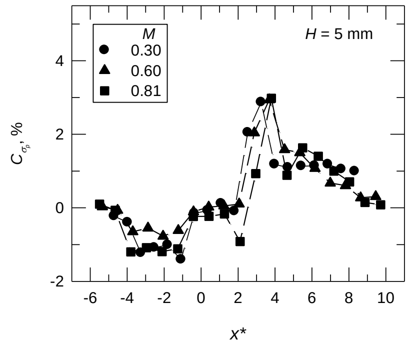

Figure 9. Distribution of fluctuating pressure coefficients for H = 5 mm.

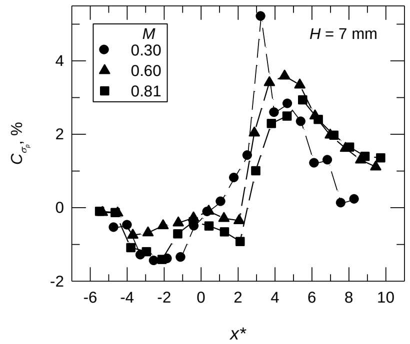

Figure 10. Distribution of fluctuating pressure coefficients for H = 7 mm.

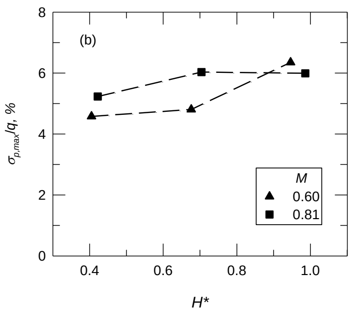

Figure 11. The maximum fluctuating pressure coefficient.

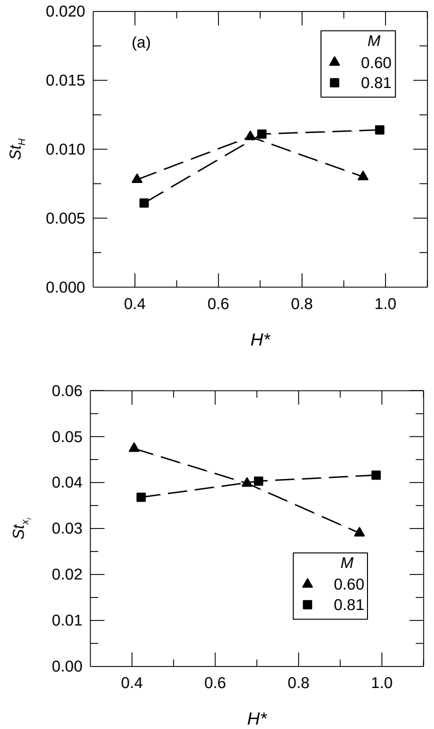

Figure 12. The effect of M and H^* on the step mode.

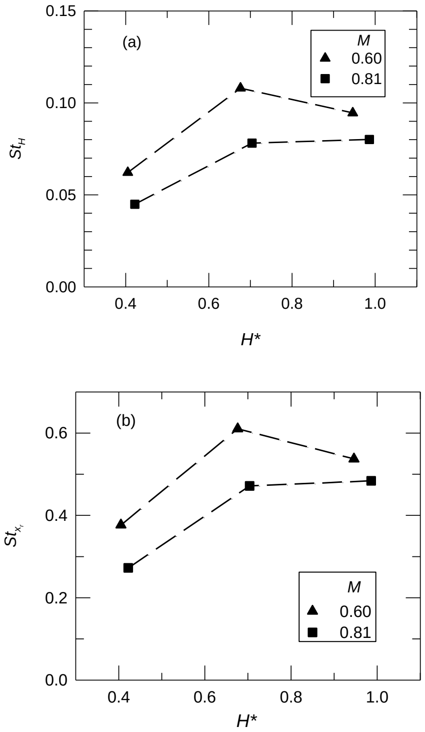

Figure 11. The effect of M and H^* on the shear layer mode.